Mineralogical Magazine, June 2013, Vol. 77(4), pp. 485–498

Spectroscopy and X-ray structure refinement of sekaninaite from Dolní Bory (Czech Republic)

F. Radica[1], F. Capitelli[2], F. Bellatreccia[1,3], G. Della Ventura[1,3,4], A. Cavallo[4], M. Piccinini[5] and F. C. Hawthorne[6]

[1] Dipartimento di Scienze Geologiche, Università degli Studi Roma Tre, Largo S. Leonardo Murialdo 1, 00146 Rome, Italy
[2] Istituto di Cristallografia, Consiglio Nazionale delle Ricerche (CNR), Via Salaria Km 29,300, 00016 Monterotondo, Rome, Italy
[3] Laboratori Nazionali di Frascati – Istituto Nazionale di Fisica Nucleare (LNF – INFN), Via E. Fermi 40, 00044 Frascati, Rome, Italy
[4] Istituto Nazionale di Geofisica e Vulcanologia (INGV), Via di Vigna Murata 605, 00143 Rome, Italy
[5] Porto Conte Ricerche s.r.l., Strada Provinciale 55 Km 8,400, 07041 Alghero, Sassari, Italy
[6] Department of Geological Sciences, University of Manitoba, Winnipeg, Manitoba R3T 2N2, Canada

[*Received 21 March 2013; Accepted 11 May 2013; AE: S. Krivovichev*]

ABSTRACT

The crystal chemistry of sekaninaite from Dolní Bory, Czech Republic, was characterized by a multi-method approach. Particular emphasis was put on the characterization of the channel constituents (i.e. H_2O and CO_2). Electron microprobe analysis shows the sample to be close to the Fe endmember [X_{Fe} = Fe/(Fe+Mg) = 94%) with significant Mn (1.48 wt.%) present; laser ablation mass-spectrometry showed the presence of 0.42 wt.% Li_2O. H_2O and CO_2 contents (1.48 and 0.17 wt.%, respectively) were determined via secondary-ion mass-spectrometry. Sample homogeneity was checked by Fourier-transform infrared (FTIR) imaging using a microscope equipped with a focal plane array detector. Single-crystal FTIR spectroscopy confirmed the presence of two types of H_2O groups in different orientations (with prevalence of the type II orientation), and that CO_2 is oriented preferentially normal to the crystallographic *c* axis. Using the Beer-Lambert relation, integrated molar coefficients, ε_i, were calculated for both types of H_2O (ε_i $H_2O^{[I]}$ = 6000±2000; ε_i $H_2O^{[II]}$ = 13000±1000) and for CO_2 (ε_i CO_2 = 2000±1000).

Keywords: sekaninaite, crystal-structure refinement, EMPA + SIMS analysis, FTIR spectroscopy

Introduction

Sekaninaite is the Fe^{2+}-dominant member of the cordierite group (Černý *et al.*, 1997). The first occurrence of this mineral was reported by Sekanina (1928) in the pegmatites of Dolní Bory; however, it was described definitively as a new mineral species by Staněk and Miškovský (1964, 1975). Cordierites are framework aluminosilicates with the ideal formula $(\square,Na)(Mg,Fe)_2Al_4Si_5O_{18}(\square,H_2O,CO_2)$ = $XM_2T_9O_{18}Y$ and form a continuous solid solution between the Mg^{2+} endmember (cordierite s.s.) and the Fe^{2+} endmember (sekaninaite). The main structural feature of these minerals is the presence of 6-fold rings of tetrahedra stacked along the *c* crystallographic axis. These rings form cavities that can accommodate large cations such as Na^+ and K^+ and molecules such as H_2O and CO_2. The sekaninaite framework can be described as a stacking of pseudo-hexagonal Si/Al layers of tetrahedra and mixed layers of tetrahedra and octahedra (Fig. 1). Alkali cations, H_2O and CO_2 fill the resulting pseudo-hexagonal channel,

* E-mail: fradica@uniroma3.it
DOI: 10.1180/minmag.2013.077.4.08

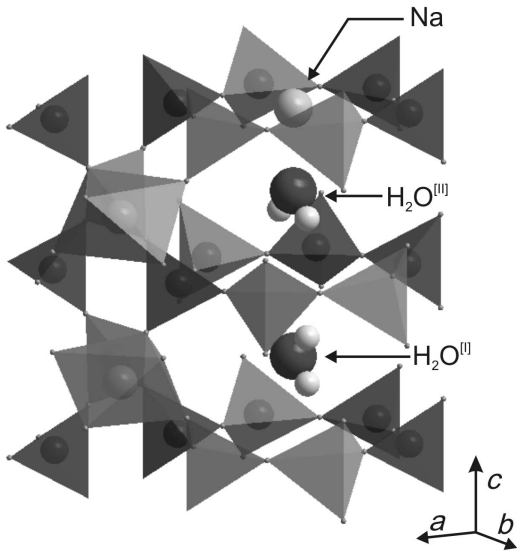

FIG. 1. Schematic view of a portion of the sekaninaite structure which includes the channel parallel along the *c* axis. Si-containing tetrahedra are shown in dark grey and Al-containing tetrahedra are shown in light grey. The structural position of Na and both orientation types of H_2O are shown in the channels.

occupying sites on the *c* axis at (0, 0, 0) for Na, and (0, 0, ¼) for H_2O and CO_2 (Hochella *et al.*, 1979; Malcherek *et al.*, 2001; Yakubovich *et al.*, 2004). The chemical composition of the framework has the ideal formula 4 Al a.p.f.u. and 5 Si a.p.f.u. Due to the high concentration of alkali cations within the channels (Černý *et al.*, 1997; Yacobuvich *et al.*, 2004), charge-balance may be restored by Be^{2+} substitution at the tetrahedrally coordinated sites (Armbruster and Irouschek, 1983; Yacobuvich *et al.*, 2004) or Li^+ at the octahedrally coordinated sites (Černý *et al.*, 1997; Gottesmann and Förster, 2004). Unlike cordierite, sekaninaite is not a widespread mineral, and usually occurs in the albite zone of pegmatitic rocks (Staněk and Miškovský, 1964; Orlandi and Pezzotta, 1994; Guastoni *et al.*, 2004). Other occurrences of sekaninaite were reported in altered bauxitic lithomarges (Ryback *et al.*, 1988) and in Fe-rich pyrometamorphosed rocks (Sharygin *et al.*, 2009; Grapes *et al.*, 2010).

Analytical methodology

The studied sample is from the type locality of Dolní Bory (Czech Republic) (Staněk and Miškovský, 1964). The grains analysed were extracted from a very clear, light blue and almost inclusion-free large crystal that gradually changes toward the rim of the sample into a greenish alteration product of clay minerals. Due to the presence of light elements (Li, H and C), the chemical composition of sekaninaite was determined using a multi-method approach. Elements from Si to K (Table 1) were analysed using a Jeol JXA 8200 WD-ED electron microprobe (EMP) at the Istituto Nazionale di Geofisica e Vulcanologia (INGV), Rome. Working conditions were: 15 kV accelerating voltage, 7 nA sample current, 5 μm beam diameter. Count times were 10 s on the peak and 5 s on the background on both sides of the peak. Standards, spectral lines and crystals used were: albite (Na*K*α, TAP), pargasite (Ca*K*α, PET), wollastonite (Si*K*α, PET), K-feldspar (K*K*α, PET), kyanite (Al*K*α, TAP), pargasite (Mg*K*α, TAP), augite (Fe*K*α,LiF), titanium oxide (Ti*K*α, LiF) and spessartine (Mn*K*α, LiF). Data correction was done using the ZAF method. Sample homogeneity was verified by collecting many points per crystal.

TABLE 1. Chemical composition (mean of five analyses) and chemical formula (a.p.f.u.), based on 18 oxygen atoms per formula unit, for the sekaninaite studied.

	Wt.%	Range		a.p.f.u.
SiO_2	45.41	45.65–45.16	Si	4.954
TiO_2	0.01	0.02–0.00	Al	4.054
Al_2O_3	31.53	31.84–31.27	ΣT	9.008
FeO	17.55	17.99–17.37		
MnO	1.48	1.52–1.39	Mg	0.079
MgO	0.48	0.53–0.46	Fe	1.602
CaO	0.03	0.05–0.02	Ti	0.001
Na_2O	0.90	0.96–0.86	Mn	0.137
K_2O	0.02	0.02–0.01	Li	0.186
Li_2O	0.42	0.43–0.41	ΣOct.	2.005
H_2O	1.48	1.54–1.38		
CO_2	0.17	0.23–0.11	Ca	0.004
Total	99.48		Na	0.190
			K	0.002
			ΣCh.	0.196
			H_2O	0.538
			CO_2	0.025

All data from EMP analysis except for Li_2O (Nano-laser ablation mass spectroscopy, Nano-LAMS), H_2O and CO_2 from SIMS (see text).

Lithium was determined by laser ablation inductively coupled plasma mass spectrometry (LA-ICP-MS) at the Department of Geological Sciences, University of Manitoba, Winnipeg, Canada, using a Merchantek New Wave UP213 laser ablation system. The data were collected from three spots with a Nd:YAG laser, beam diameter of 50 μm, 10 Hz repetition rate, ~5 J/cm^2 fluence, 30 s background acquisition and 50 s ablation time. Li was standardized against NIST SRM 610.

H_2O and CO_2 were quantified by secondary-ion mass spectrometry (SIMS) using a Cameca IMS4f ion microprobe at the Edinburgh Materials and Micro Analysis Centre, University of Edinburgh. Sputtered secondary ions ^{1}H, ^{12}C and ^{28}Si were measured with an energy offset of 75 V and an energy window of 19 eV, under operating conditions of 4500 V secondary-beam voltage and 8 nA and 10 kV for the primary beam of O^- ions. Under these conditions, the primary-ion beam sputters an elliptical area with long diameter 25−30 μm and maximum depth of 3 μm. All analyses involved a 3 minute burn-in time followed by 20 cycles of 5 s counts for each isotope. The mean isotope ratios ^{1}H/^{28}Si and ^{12}C/^{28}Si for the last 10 cycles in each analysis were taken as the final results in order to avoid surface contamination. Analyses expressed as isotopic ratios of ^{1}H/^{28}Si and ^{12}C/^{28}Si were converted to wt.% H_2O or CO_2 by comparison with the calibration lines produced from fitting two standards analysed several times throughout the same analytical session. The standards used were the samples ANMH (X_{Mg} = 0.89; H_2O = 1.54 wt.%; and CO_2 = 0.7 wt.%, Thompson *et al.*, 2001) and 8/90 (labelled 81−90 X_{Mg} = 0.75; H_2O = 0.81%; and CO_2 = 1.31 wt.%, Thompson *et al.*, 2001).

X-ray diffraction data were collected at the Istituto di Cristallografia, Bari, with a Nonius Kappa CCD area-detector diffractometer (Table 2); data collection: *COLLECT* (Nonius, 1998); cell refinement and data reduction: *EvalCCD* (Duisenberg *et al.*, 2003), absorption correction: *SADABS* (Sheldrick, 2008). The structure was solved through the Direct Methods procedure of *SIR2008* (Burla *et al.*, 2007) in the

TABLE 2. Crystal data and structure-refinement data for sekaninaite from Dolní Bory.

Temperature	293(2) K
Radiation, Wavelength	Mo-*K*α, 0.71073 Å
Crystal system	Orthorhombic
Space group	*Cccm*
Unit-cell dimensions	a = 17.2340(15) Å
	b = 9.8457(18) Å
	c = 9.3463(18) Å
Volume	1585.9(4) Å^3
Z	16
Calculated density	2.726 Mg m^{-3}
Absorption coefficient	2.315 mm^{-1}
F(000)	1279
Crystal size (mm)	0.25 × 0.25 × 0.12
Theta range for data collection	5.25º to 27.52º
Limiting indices	$-22 \leqslant h \leqslant 22$, $-12 \leqslant k \leqslant 12$, $-12 \leqslant l \leqslant 10$
Reflections collected / unique	9441 / 942 [R_{int} = 0.0297]
Completeness to theta	96.6 % (theta = 27.52º)
Max. and min. transmission	0.7686 and 0.5953
Refinement method*	Full-matrix least-squares on F^2
Data / restraints / parameters	942 / 1 / 84
Goodness-of-fit on F^2	1.162
Final R indices [I>2σ(I)]	R_1 = 0.0178, wR_2 = 0.0490
R indices (all data)	R_1 = 0.0186; wR_2 = 0.0499
Extinction coefficient	0.0092(4)
Largest diff. peak and hole	0.348 and –0.416 e Å^{-3}

* *SHELXL-97* weighting scheme applied: $w^{-1} = [\sigma^2(F_o^2) + (0.0179P)^2 + 3.4870P]$, where $P = [(F_o^2 + 2F_c^2)/3]$.

orthorhombic space group *Cccm* (n. 66), with the following unit-cell constants: a = 17.2340(15), b = 9.8457(18), c = 9.3463(18) Å, and refined by full-matrix least-squares based on F^2, *SHELXL-97* (Sheldrick, 2008); final R indices were, for [$I>2\sigma(I)$] R_1 = 0.0178 and wR_2 = 0.0490, and for all data R_1 = 0.0186 and wR_2 = 0.0499.

Micro-Raman spectra were collected at Porto Conte Ricerche s.r.l., Alghero (Sassari), using a Bruker Senterra Raman microscope equipped with a 532 nm laser operated at 50 mW; 10 acquisitions of 5 s each were accumulated, with a spectral resolution set at 3 to 5 cm^{-1} (100× lens, NA = 0.9). Raw data were slightly smoothed.

The FTIR spectra were acquired using a Nicolet Magna 760 spectrophotometer, equipped with a NicPlan Microscope, a KBr beamsplitter and a liquid nitrogen-cooled MCT detector at the Dipartimento di Scienze Geologiche, Università Roma Tre. The polarized spectra were collected using a gold-wire-grid polarizer on a ZnSe substrate. The nominal resolution is 4 cm^{-1} and 128 scans were averaged for both spectrum and background. The samples for polarized IR measurements were oriented using a polarizing microscope equipped with a spindle-stage; the program *ExcalibrW* (Bloss, 1981; Gunter *et al.*, 2005) was used to process the extinction data and to determine the 2V values. The oriented fragments were transferred to glass slides and doubly polished to thickness <100 μm. Sample thickness was checked with a Leica DCM 3D optical profilometer at the Laboratorio Interdipartimentale di Microscopia Elettronica (LIME), Università Roma Tre. The nominal vertical resolution was <15 nm in confocal mode (20× lens, NA = 0.50) and <4 nm in interferometric mode (50× lens, NA = 0.50); sample thickness was averaged for the whole surface of the slab.

The FTIR images were collected at the Laboratori Nazionali di Frascati-Istituto Nazionale di Fisica Nucleare (LNF-INFN,) Frascati (Rome) using a Bruker® Hyperion 3000 IR microscope equipped with a 64 × 64-pixel focal-plane array (FPA) of liquid nitrogen-cooled MCT detectors. Using a 15× objective, each image covers an area of 170 μm × 170 μm with a nominal spatial resolution of et al., 2010). The nominal resolution was set at 4 cm^{-1} and 64 scans were averaged for each spectrum and background.

Refractive indexes were determined by the double-variation method (Su *et al.*, 1987; Gunter *et al.*, 2004) using standard Cargille liquids as reference.

Chemical composition

Selected micro-chemical data for the sample studied are reported in Table 1. Fe_{tot} was considered as Fe^{2+}. The chemical formula, based on 18 oxygen atoms p.f.u., is $Na_{0.19}(Mg_{0.08}Fe_{1.60}Mn_{0.14}Li_{0.19})Al_{4.05}Si_{4.95}O_{18}\cdot 0.54H_2O\cdot 0.03CO_2$. The chemical composition of the analysed sample is close to those reported for other samples from the same area (Staněk and Miškovský, 1964; Hochella *et al.*, 1979; Černý *et al*., 1997). Sekaninate from Dolní Bory, like in other pegmatite assemblages, has relatively large contents of Mn, Na and Li; on the other hand it has small concentrations of Ti, Mg and K, elements usually abundant in paralava assemblages (Sharygin *et al.*, 2009; Grapes *et al.*, 2010). The Al/Si ratio is almost stoichiometric (4/5) and thus additional tetrahedrally coordinated cations are unlikely to be present. Although we do not have any information on the Fe oxidation state, we can reasonably consider all iron to be divalent, following Černý *et al*. (1997), who determined, *via* Mössbauer spectroscopy, that the $Fe^{3+}/\Sigma Fe$ is 0.5% or less for sekaninaites from the same area. Fe^{2+} is the main constituent at the octahedrally coordinated M site. Significant quantities of Li^+ (0.186 a.p.f.u.) and Mn^{2+} (0.137 a.p.f.u.) are also present, whereas Mg^{2+} and Ti^{4+} concentrations are very low. Charge imbalance due to Na^+ in the channels is compensated by Li^+ at the M site. If we consider the sum of channel-cation charges $(\Sigma_{Channel})/(Li + Be)$ ratio, we clearly see that our sample is located much closer to the 1:1 line compared to the samples analysed by Černý *et al*. (1997) (Fig. 2). The SIMS data show that the sample is almost CO_2-free and significantly enriched in H_2O, as reported by previous authors (Yakubovich *et al.*, 2004; Malcherek *et al.*, 2001; Salkress and Bloss, 1980).

Single-crystal X-ray results

X-ray structure-refinement data are reported in Table 2, atom coordinates and equivalent isotropic-displacement parameters are reported in Table 3; bond lengths are reported in Table 4. The a and b parameters (Table 2) are in line with those reported for samples from the same locality (Hochella *et al.*, 1979; Selkregg and Bloss,1980; Malcherek *et al.*, 2001) and with those of

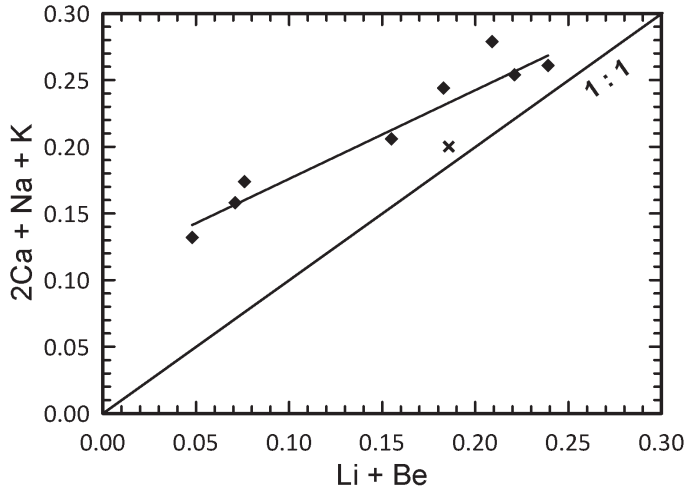

FIG. 2. Sum of channel cation charges *vs.* Be + Li charges. ×: this work, ◆: samples from Dolní Bory (Černý *et al*., 1997); the regression line for these latter samples is reported.

synthetic iron-cordierite (Borbeski and Schreyer, 1990; Bulbak and Shvedenkova, 2011), whereas the *c* parameter (and consequently the cell volume) is at least 0.03 Å greater, a value that is more typical of Mg-cordierite. Parameters that, in our case, may increase the *c* parameter are the

TABLE 3. Wyckoff site, atom coordinates, equivalent-displacement parameters ($Å^2$), and site-occupancy factors (SOF) of sekaninaite from Dolní Bory.

Site	Wyckoff symbol	*x/a*	*y/b*	*z/c*	U_{eq}	s.o.f.
*T*1	*4b*	0	½	¼	0.0136(2)	
*T*2	*8l*	0.18999(4)	0.07921(7)	0	0.01273(17)	
*T*3	*8l*	0.13471(4)	0.76594(7)	0	0.01270(17)	
*T*4	*8k*	¼	¼	0.25011(8)	0.01421(18)	
*T*5	*8l*	0.04972(4)	0.30757(7)	0	0.01298(18)	
M	*8g*	0.33688(2)	0	¼	0.01448(18)	0.873(5) Fe + 0.035(5) Mg + 0.09 Li*
O1	*16m*	0.24402(7)	0.89508(12)	0.35809(13)	0.0166(3)	
O2	*16m*	0.06074(7)	0.58523(13)	0.34885(14)	0.0165(3)	
O3	*16m*	0.82705(7)	0.69477(12)	0.35782(14)	0.0167(3)	
O4	*8l*	0.04328(10)	0.7543(2)	0	0.0210(4)	
O5	*8l*	0.11931(10)	0.18336(19)	0	0.0209(4)	
O6	*8l*	0.16213(10)	–0.07670(18)	0	0.0204(4)	
O7	*8g*	0.0580(6)	0	¼	0.069	0.03*
O8w	*4a*	0	0	¼	0.101(6)	0.62(3) O + 0.03* C
Na	*4c*	0	0	0	0.035(4)	0.203(10)

Equivalent isotropic *U* is defined as 1/3 of the trace of the orthogonalized U_{ij} tensor.
Na and O8w refined with isotropic displacement parameters.
C and O7 isotropic displacement parameters fixed at Malcherek *et al.* (2001) values.
* s.o.f. fixed for Li at nano-LAMS (Table 1) and for CO_2 at SIMS (Table 1) values.

TABLE 4. Selected bond lengths (Å) for sekaninaite from Dolní Bory.

*T*1–O2	1.6289(12)	*M*–O1[1]	2.1561(12)
*T*1–O2[10]	1.6289(12)	*M*–O1[2]	2.1561(12)
*T*1–O2[1]	1.6289(12)	*M*–O2[3]	2.1613(12)
*T*1–O2[11]	1.6289(12)	*M*–O2[4]	2.1613(12)
<*T*1–O>	1.6289	*M*–O3[5]	2.1729(13)
*T*2–O5	1.5923(18)	*M*–O3[6]	2.1729(13)
*T*2–O6	1.6084(19)	<M–O>	2.1635
*T*2–O1[1]	1.6402(13)		
*T*2–O1[9]	1.6402(13)	*Na*–O8w[16]	2.3366(5)
<*T*2–O>	1.6203	*Na*–O8w	2.3366(5)
*T*3–O4	1.5799(18)	*Na*–O4[8]	2.532(2)
*T*3–O6[12]	1.6198(19)	*Na*–O4[2]	2.532(2)
*T*3–O3[13]	1.6404(13)	*Na*–O7[16]	2.541(4)
*T*3–O3[14]	1.6404(13)	*Na*–O7[15]	2.541(4)
<*T*3–O>	1.6201	*Na*–O7[17]	2.541(4)
*T*4–O3[7]	1.7528(13)	*Na*–O5[16]	2.7363(19)
*T*4–O3[5]	1.7528(13)	<*Na*–O>	2.512
*T*4–O1[3]	1.7532(13)		
*T*4–O1[1]	1.7532(13)	C–O7[15]	0.999(10)
<*T*4–O>	1.7530	C–O7	0.999(10)
*T*5–O5	1.7128(19)	*Na*–C1[16]	2.3366(5)
*T*5–O4[8]	1.7146(18)	O7–O8w	0.999(10)
*T*5O2[1]	1.7736(13)		
*T*5–O2[9]	1.7736(13)		
<*T*5–O>	1.7437		

Symmetry operators: #1 *x*,–*y*+1,–*z*+1/2; #2 *x*,*y*–1,*z*; #3 –*x*+1/2,*y*–1/2,–*z*+1/2; #4 –*x*+1/2,–*y*+1/2,*z*; #5 *x*–1/2,*y*–1/2,*z*; #6 *x*–1/2,–*y*+1/2,–*z*+1/2; #7 *x*+1/2,*y*–1/2,*z*; #8 *x*,–*y*,–*z*+1/2; #9 –*x*+1,–*y*+1,*z*; #10 –*x*,–*y*+1,–*z*; #11 *x*,–*y*+1,*z*–1/2; #12 –*x*,*y*,–*z*+1/2; #13 –*x*,–*y*+1,*z*; #14 *x*–1/2,*y*+1/2,*z*; #15 *x*,*y*+1,*z*; #16 –*x*+1,*y*,*z*–1/2; #17 –*x*+1,*y*,–*z*+1/2.

absence of Be at the *T* sites (see below) (Yakubovich *et al.*, 2004) and the presence of H_2O and CO_2 (Table 1) in the channels (Armbruster and Bloss, 1982).

In sekaninaite, the framework consists of five *T* tetrahedra (Cohen *et al.*, 1977; Armbruster, 1986). Three *T* sites (*T*2, *T*3 and *T*5) form the six-membered pseudo-hexagonal ring and the remaining two *T* sites (*T*1 and *T*4) connect the rings into a chain which extends parallel to the *c* crystallographic axis. Aluminium occupies the *T*4 and *T*5 sites (two of the six tetrahedra of the ring are occupied by Al) and the remaining sites (*T*1, *T*2 and *T*3) are occupied by Si (Fig. 1). Beryllium, if present, occurs usually at the *T*4 site, according to the substitution $Na^{+} + Be^{2+} \rightarrow Al^{3+}$. This substitution leads to a decrease of the mean *T*4−O distance (Table 4) as observed by Armbruster (1986). On the other hand, substitution of Mg for Fe leads to shortening of the *T*4−O distance (Malcherek *et al.*, 2001). Figure 3 shows the *T*4−O distances from various refinements in the literature as a function of X_{Mg} (Fig. 3*a*) and Be at the *T*4 site (wt.%) (Fig. 3*b*); samples with >1% Be at the *T*4 site (corresponding to ~0.02 a.p.f.u.) are represented by circles. As we may observe from Fig. 3*a*, samples with large Be values at *T*4 tend to deviate from the trend described by the $Fe^{2+} \rightarrow Mg^{2+}$ substitution, leading to a decrease in the *T*4−O bond length; this trend is evident in Fig. 3*b*. The *T*4−O bond length for our sample is reported in Fig. 3*b* as a dashed line; we may reasonably infer that Be in the sample is <0.02 a.p.f.u. This conclusion is also corroborated by Fig. 2.

All atoms were refined with anisotropic-displacement parameters, with the exception of Na and O8w which were refined with isotropic-displacement parameters, and of C and O7 (for CO_2) whose isotropic-displacement parameters were fixed at values compatible with ferromagnesian cordierite (Malcherek *et al.*, 2001); the site-occupancy factor (s.o.f.) for Li at the *M* site was fixed at the nano-LAMS value for Li

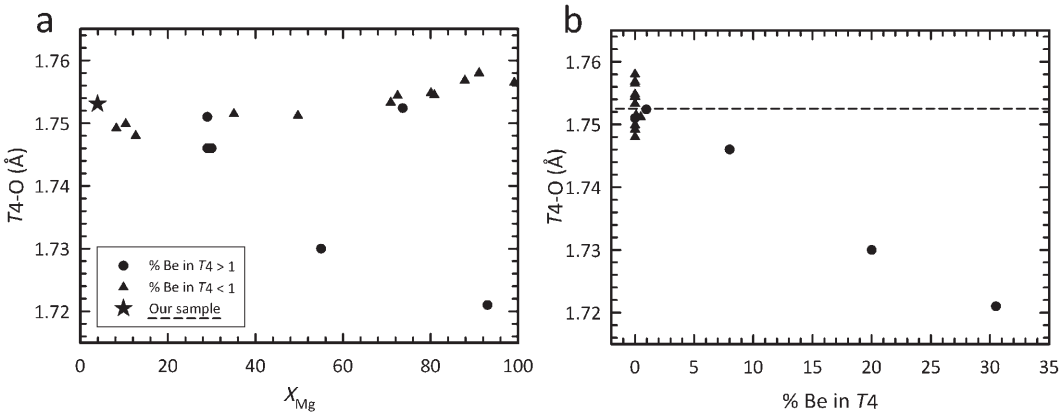

FIG. 3. *T*4–O bond lengths for various cordierite samples *vs.* (*a*) the magnesium number (X_{Mg}) and (*b*) the % Be at the *T*4 site. Triangles indicate the samples with % Be in *T*4 > 1; the star and the dashed line represents our sample. Data from Hochella *et al.* (1979), Armbruster *et al.* (1986), Malcherek *et al.* (2001) and Yakubovich *et al.* (2004).

(Table 1); Fe and Mg were refined, constraining the sum of their occupancies to be equal to (1 − Li); s.o.f. were refined for Na and H_2O in the channels, and the CO_2 occupancy was fixed at the SIMS value. As previously stated, the lack of monovalent charge at the *M* site due to the presence of Li^+, is counter-balanced by the presence of Na^+ in the channel; H atoms of the H_2O group could not be detected due to the low concentration of H_2O in the sample (Table 1); the Fe s.o.f. value is slightly over-estimated due to the contribution of Mn. Further details of the crystal structure refinements can be obtained from the Fachinformations-zentrum Karlsruhe, 76344 Eggenstein-Leopoldshafen, Germany, (fax: +49 7247-808-666; e-mail: crysdata@fiz-karlsruhe.de) on quoting the depository number CSD-425930. The crystallographic information file (comprising bond distances) and tables of structure factor data have been deposited with the Principal Editor at http://www.minersoc.org/pages/e_journals/dep_mat_mm.html. The list of F_o/F_c data is available from the author up to one year after the publication has appeared.

Optical properties

The studied sekaninaite is biaxial negative. The measured $2V_\alpha$ value is 64±2º, refractive indexes are α = 1.5640(4), β = 1.5740(4) and γ = 1.5784(4). These values are slightly lower (by 0.004) than those reported by Salkregg and Bloss (1980), probably due to larger H_2O and Fe contents in the latter.

FTIR spectroscopy

The single-crystal unpolarized IR spectrum of sekaninaite (Fig. 4) can be divided into two main regions: (I) 3900−3300 cm^{-1} where absorption bands are due to H_2O stretching modes (Goldman *et al.*, 1977), and (II) 2600−2000 cm^{-1} where absorption bands are related to the antisymmetric stretching mode of CO_2. As shown by Geiger and Kolesov (2002) and Della Ventura *et al.* (2009, 2012) for CO_2-rich samples, the combination modes of CO_2 are also observed, overlapping with H_2O bands in region I. Additional peaks due to H_2O modes also occur around 1600 cm^{-1} (bending) and 5250 cm^{-1} (combination) (Della Ventura *et al.*, 2012).

The polarized spectra in the 4000−3200 cm^{-1} range are given in Fig. 5*a* (right). Where the electric vector **E** is parallel to the crystallographic axis *c* (**E**||*c*), two sharp peaks are observed, the more intense centred at 3575 cm^{-1}, and the weaker at 3689 cm^{-1}. The **E**||*b* spectrum has a very broad peak at ~3630 cm^{-1} with a pronounced shoulder at 3575 cm^{-1}. The **E**||*a* spectrum shows a broad and very weak multi-component absorption with maxima at 3630 cm^{-1} and 3595 cm^{-1}.

The polarized spectra in the 5300−5200 cm^{-1} range (Fig. 5*a*, left) show a fairly sharp peak at 5266 cm^{-1} for **E**||*c*, and a broader peak at ~5250 cm^{-1} for **E**||*b*. The **E**||*a* spectrum is featureless.

In region II of the spectrum (Fig. 5*b* left), only a weak peak at 2348 cm^{-1} is observed for **E**||*a*. Outside these ranges, additional relevant peaks

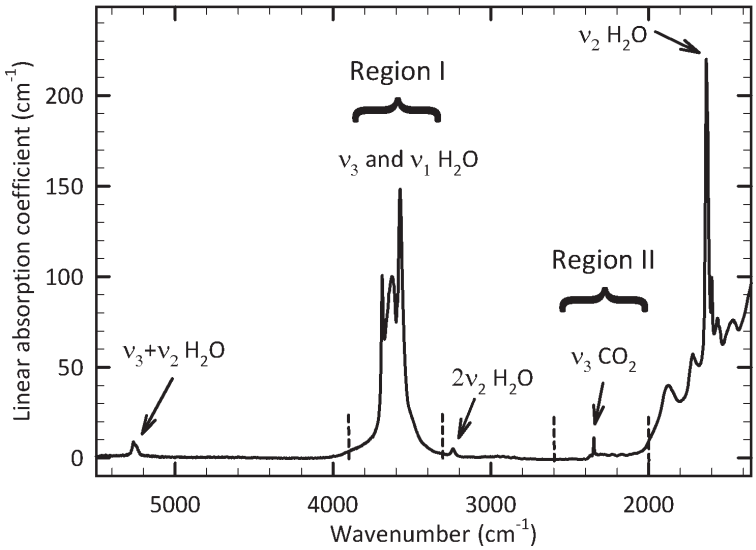

FIG. 4. Single-crystal unpolarized-light IR spectrum of sekaninaite. The two regions from 3900 to 3300 cm^{-1} and from 2600 to 2000 cm^{-1} are highlighted. The H_2O bending mode at 1635 cm^{-1}, the H_2O bending first overtone mode at 3241 $cm^{-1}$and the H_2O combination mode at ~5260 cm^{-1} are indicated by arrows.

are observed in **E**||*c* at 3241 cm^{-1} (Fig. 5*a* right) and 1635 cm^{-1} (Fig. 5*b* right). A triplet of very weak components is finally observed at 1552, 1600 and 1635 cm^{-1} polarized for **E**||*a* and **E**||*b*. Note that the peak at 1635 cm^{-1} is probably offscale due to detector saturation, even for a slab thickness <50 μm.

The FPA images of selected sample areas were collected to check for possible inhomogeneity in the volatile distribution across the studied crystals (Della Ventura *et al.*, 2012). Figure 6 shows that there is no significant variation in the H_2O contents for the whole sample. Imaging of CO_2 distribution was not possible because the CO_2 anti-symmetric stretching peak could not be distinguished from the noise in the FPA data due to the low concentration of CO_2. However CO_2 homogeneity was checked by collecting several random spots on the slab, and the results always gave the same value within estimated standard deviation.

FTIR band assignment

Although there are several spectroscopic (FTIR + Raman) works on the channel volatile constituents of Mg-rich cordierite in the literature (Goldman *et al.*, 1977; Geiger and Kolesov, 2002; Della Ventura *et al*., 2009, 2012), polarized data for Fe-rich cordierite are rare (Kolesov and Geiger, 2000). According to these works, it is now well established that extra-framework H_2O groups occur in the structural channels of cordierite with the molecular plane parallel to (100). However, H_2O can be oriented in two different ways: type I H_2O (hereafter $H_2O^{[I]}$) has its H−H vector oriented parallel to the *c* axis, and type II H_2O ($H_2O^{[II]}$) has its H−H vector parallel to the *b* axis. H_2O groups of the latter type are bonded to locally associated channel Na cations as in beryl (Hawthorne and Černý, 1977; Sherriff *et al.*, 1991). The linear CO_2 molecules are oriented parallel to the crystallographic *a* axis (Khomenko and Langer, 2005; Aines and Rossman, 1984).

The band assignment given below follows the criteria proposed by Goldman *et al.* (1977), Geiger and Kolesov (2002) and Della Ventura *et al*., (2009), based on single-crystal infrared polarized-light determination on oriented slabs of Mg-rich cordierite. However, as we will see from the band positions and polarization behaviour, these criteria are also suitable for sekaninaite.

The peak at 3689 cm^{-1} (Fig. 5*a* right), polarized for **E**||*c*, is assigned to the anti-symmetric stretching mode ν_3 of $H_2O^{[I]}$; the corresponding symmetric stretching mode (ν_1) in Mg-cordierite is observed at 3595 cm^{-1} (Paukov *et al.*, 2007) and is polarized for **E**||*b*. In the

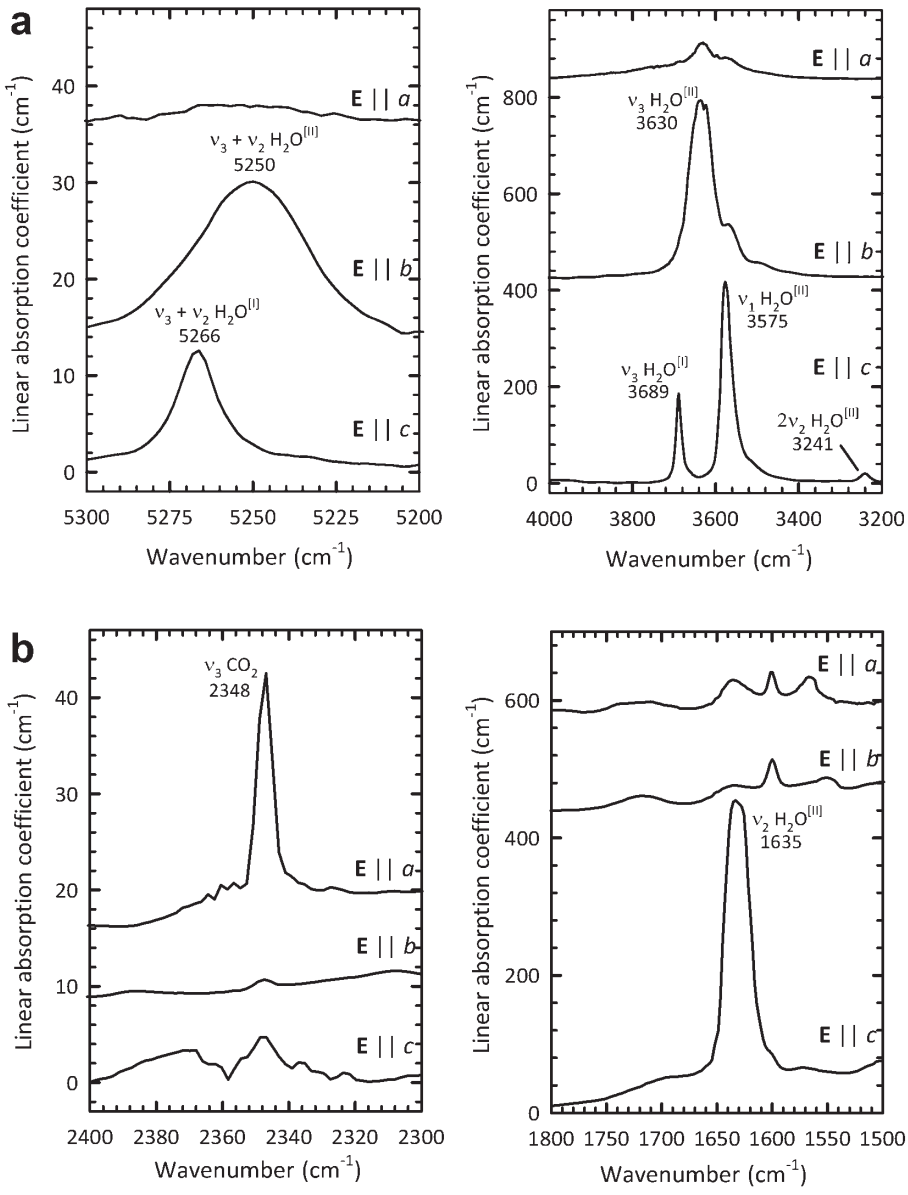

FIG. 5. (*a*). Single-crystal polarized-light IR spectra of sekaninaite in the ranges 5300−5200 cm^{-1} (left) and 4000−3200 cm^{-1} (right). Spectra were collected on (010) 43 μm thick and (100) 47 μm thick oriented slabs. (*b*) Single-crystal polarized-light IR spectra of sekaninaite in the CO_2 antisymmetric stretching mode region (left) and $H_2O^{[II]}$ bending mode (right). Spectra were collected on the same slabs of Fig. 3*b* except for the **E**||*b* spectrum, which was collected from a (001) 168 μm thick slab.

spectra collected for sekaninaite studied here, this component cannot be resolved due to the very high intensity of the 3630 cm^{-1} peak (Fig. 5*a*). The broad band at 3630 cm^{-1} polarized in **E**||*b* is assigned to the antisymmetric stretching mode ν_3 of $H_2O^{[II]}$. The corresponding symmetric stretching band ν_1 occurs at 3575 cm^{-1} in **E**||*c*. The weak absorptions at 3575 cm^{-1} in **E**||*b* and

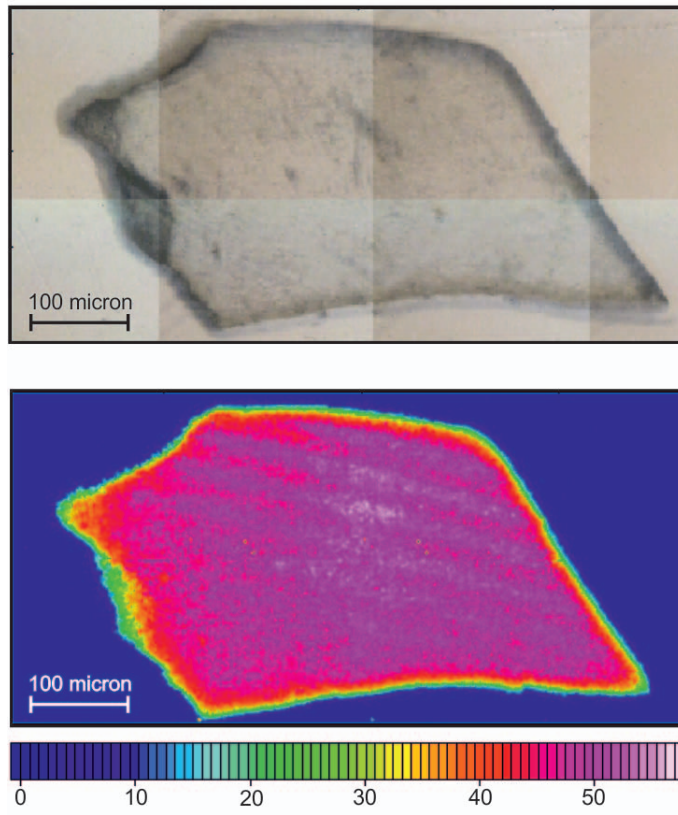

FIG. 6. FTIR image of the (100) section, 47 μm thick slab of sekaninaite. Above: video image of the sample. Below: FPA image of the same sample; integration of the H_2O stretching bands in the range 3500−3700 cm^{-1}. The chromatic scale is proportional to volatile contents, units are arbitrary.

3630 cm^{-1} in **E**||*a* (Fig. 5*a*) can be due to slight tilting during sample preparation; the latter could be also ascribed to a very small amount of H_2O with its H−H vector parallel to *a* (Kolesov and Geiger, 2000). A peak at 3595 cm^{-1} observed in **E**||*a* was assigned by Della Ventura *et al.* (2009, 2012) to the $\nu_3 + 2\nu_2$ combination mode of CO_2. In the present case, because of the very small concentration of CO_2, the assignment must be different; the band is probably due to minor tilting of the slab.

The bending mode ν_2 of $H_2O^{[II]}$ is observed at 1635 cm^{-1} (Fig. 5*b*, right) and is polarized parallel to the *c* axis (Goldman *et al.*, 1977; Della Ventura *et al.*, 2009); the same behaviour is observed for its first overtone mode (Fig. 5*a*, right) at 3241 cm^{-1} (Herzberg, 1956). On the other hand, the bending mode ν_2 of $H_2O^{[I]}$ is much less intense and occurs as three features centred at 1552, 1600 and 1635 cm^{-1} as already observed by Goldman *et al.* (1977). The assignment of these features to H_2O modes is supported by the fact that they are absent in samples with small water contents (Della Ventura *et al.*, 2012) and by the fact that they disappear with the other fundamental modes after dehydration (Goldman *et al.*, 1977). The bending mode of $H_2O^{[I]}$ is expected to be polarized for **E**||*b* though they also appear for **E**||*a* (see also Goldman *et al.*, 1977).

In the near-infrared (NIR) region (Fig. 5*a*, left), the ($\nu_3 + \nu_2$) combination modes at 5266 cm^{-1} (for $H_2O^{[I]}$) and at 5250 cm^{-1} (for $H_2O^{[II]}$) are polarized with **E**||*c* and **E**||*b*, respectively, as is also observed for Mg-cordierite (Goldmann *et al.*, 1977; Della Ventura *et al.*, 2012).

The ν_3 anti-symmetric stretching vibration mode of CO_2 (Fig. 5*b*, left) at 2348 cm^{-1} is fully polarized for **E**||*a*.

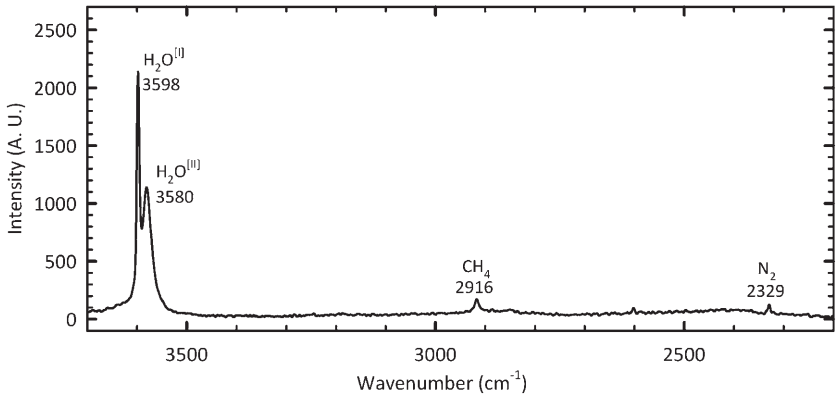

FIG. 7. Background-corrected Raman spectrum of sekaninaite. The symmetric stretching modes for both types of H_2O are indicated; intensity in arbitrary units.

Unpolarized Raman spectroscopy

In region I (Fig. 7), two absorptions are observed: one sharp peak at 3598 cm^{-1} and a second broader peak at ~3580 cm^{-1}. The former is related to the symmetric stretching mode ν_1 of $H_2O^{[I]}$ and the latter to the ν_1 mode of $H_2O^{[II]}$ (Kolesov and Geiger, 2000). No bands are present in the Raman spectrum at 1383 cm^{-1} where the CO_2 symmetric stretching should be located (Kolesov and Geiger, 2000), in accord with the very small amount of CO_2 in the crystal studied. However, two weak absorptions are resolved at 2329 cm^{-1}, indicating the presence of N_2 and at 2916 cm^{-1}, indicating the presence of CH_4 (Cesare *et al.*, 2007) in the sample.

Calibration of molar absorption coefficients of H_2O and CO_2 in sekaninaite

The Beer-Lambert law, $C = A/(t \cdot \varepsilon)$, can be used to quantify H_2O and CO_2 from polarized FTIR spectroscopy in cordierite (Della Ventura *et al.*, 2009, 2012). In this relation, the molar absorption coefficient ε is matrix specific and must be calibrated by combining the spectroscopic measurements with a second independent analytical method. Rearranging the above equation, $\varepsilon = (A \cdot k)/(t \cdot D \cdot C)$, where C (wt.%) is the concentration of the target molecule, A is the infrared absorbance, t is the slab thickness in cm, D is the value of the sample density (g/cm^3) and k is a conversion factor needed to convert from wt.% to mol l^{-1}; for H_2O, k = 1.8 (Beran *et al.*, 1993) and for CO_2, k = 4.401 (Della Ventura *et al.*, 2009). C (wt.%) was determined using SIMS, and the absorbance A was calculated as the total integrated absorbance A_i (cm^{-1}) = $A_x + A_y + A_z$, where A_x, A_y and A_z are the integrated absorptions in each polarization direction (Libowitzky and Rossman, 1996). The peak areas were obtained for each component using the data calculation routine built into the spectrometer software; the background was modelled as linear. Using this method, it is possible to quantify as little as a few ppm of H_2O or CO_2 in the sekaninaite channels, and also to distinguish the two different types of H_2O groups ($H_2O^{[I]}$ and $H_2O^{[II]}$) in a reliable way (Della Ventura *et al.*, 2012). Integrated molar coefficients for both types of H_2O were calculated using the method described in Della Ventura *et al.* (2012), calculating the concentration of $H_2O^{[II]} = 2 \cdot (Na,K,Ca)_{channel}$ from the chemical analysis of Table 1 and deriving $H_2O^{[I]} = H_2O^{tot} - H_2O^{[II]}$. Molar absorption values were thus obtained for both the principal and combination modes (Table 5). It is worth recalling here that the use of the combination modes, where applicable, is very useful as these absorptions can be measured on thicker (and thus easy to prepare) crystal slabs. The error σ_ε associated with ε was obtained using the classical statistics of error propagation (Bellatreccia *et al.*, 2005); the error on A is ~10% (Libowitzky and Rossman, 1997), the sample thickness uncertainty was set to 2 μm, the standard deviation of the density (D) is 2% and the accuracy of the SIMS analysis is better than 10%. Final values are $\varepsilon_{i\,H_2O[I]}$ = 6000±2000; $\varepsilon_{i\,H_2O[II]}$ = 13000±1000 and $\varepsilon_{i\,CO_2}$ = 2000±1000). Used in the Beer-Lambert relation, these coefficients allow us to quantify H_2O and CO_2 in Fe-rich cordierite from polarized FTIR measurements.

TABLE 5. Integrated (ε_i) and linear (ε_l) absorption coefficients of H_2O and CO_2 for sekaninaite from Dolní Bory.

		ε_i (l/mol·cm^2)	ε_l (l/mol·cm)
ν_3	$H_2O^{[I]}$ (3689 cm^{-1})+ $H_2O^{[II]}$ (3630 cm^{-1})	11000±1000	230±20
	$H_2O^{[I]}$ (3689 cm^{-1})	6000±2000	400±100
	$H_2O^{[II]}$ (3630 cm^{-1})	13000±1000	190±20
$\nu_3 + \nu_2$	$H_2O^{[I]}$ (5266cm^{-1})+ $H_2O^{[II]}$ (5250 cm^{-1})	360±40	11±1
	$H_2O^{[I]}$ (5266cm^{-1})	500±200	25±9
	$H_2O^{[II]}$ (5250 cm^{-1})	300±30	7.1±0.8
ν_3	CO_2 (2348 cm^{-1})	2000±1000	300±200

Conclusions

Polarized FTIR spectroscopy shows the presence of two types of H_2O groups in the structural channels; in particular, due to the relatively high concentration of extraframework alkali cations, $H_2O^{[II]}$ is dominant over $H_2O^{[I]}$. The FPA images of several samples show that the sample from Dolní Bory has an homogeneous H_2O distribution, unlike most cordierites where many different factors such as fractures, inclusions and secondary alteration may cause very strong inhomogeneity in H_2O concentration across a crystal (Della Ventura *et al.*, 2012). Sekaninaite from Dolní Bory contains small amounts of CO_2 and, as shown by Raman spectra, trace amounts of N_2 and CH_4.

The integrated molar absorption coefficients ε for H_2O are very close to those reported for Mg-rich cordierite by Della Ventura *et al.* (2012). On the other hand, the values of $\varepsilon_{i\ CO_2}$ obtained here cannot be considered very reliable because of the uncertainty of the SIMS value (which is more than the 50%). However, this value is close to that obtained by Della Ventura *et al.* (2006) from a CO_2-poor cordierite. This suggests that the molar coefficient of CO_2 may be dependent on bulk concentration; however, this point needs additional experimental evidence for absolute confirmation.

Acknowledgements

The authors thank Mr Renato Pagano for providing the sample studied, Vincenzo Mangione for help with the optical profilometer, Giuseppe Chita (IC-CNR, Bari) for X-ray data collection and Simon Harley (University of Edinburgh) for providing the SIMS data for H and C.

References

Aines, R.D. and Rossman, G.R. (1984) The high temperature behavior of water and carbon dioxide in cordierite and beryl. *American Mineralogist*, **19**, 319–327.

Armbruster, T. (1986). Role of Na in the structure of low-cordierite: A single-crystal X-ray study. *American Mineralogist*, **71**, 746–757.

Armbruster, T. and Bloss, F.D. (1982) Orientation and effects of channel H_2O and CO_2 in cordierite. *American Mineralogist*, **67**, 284–291.

Armbruster, T. and Irouschek, A. (1983) Cordierites from the Lepontine Alps: Na + Be → Al substitution, gas content, cell parameters and optics. *Contributions to Mineralogy and Petrology*, **82**, 389–396.

Bellatreccia, F., Della Ventura, G., Ottolini, L., Libowitzky, E. and Beran, A. (2005) The quantitative analysis of OH in vesuvianite: a polarized FTIR and SIMS study. *Physics and Chemistry of Minerals*, **32**, 65–76.

Beran, A., Langer, K. and Andrut, M. (1993) Single crystal infrared spectra in the OH range fundamentals of paragenetic garnet, omphacite and kyanite in an eclogitic mantle xenoliths. *Mineralogy and Petrology*, **48**, 257–268.

Bloss, F.D. (1981). *The Spindle Stage: Principles and Practice*. Cambridge University Press, Cambridge.

Boberski, C. and Schreyer, W. (1990) Synthesis and water contents of Fe^{2+}-bearing cordierites. *European Journal of Mineralogy*, **2**, 565–584.

Bulbak, T.A. and Shvedenkova, S.V. (2011) Solid solutions of (Mg, Fe^{2+})-cordierite: Synthesis, water content, and magnetic properties. *Geochemistry International*, **49**, 391–406.

Burla, M.C., Caliandro, R., Camalli, M., Carrozzini B., Cascarano, G.L., De Caro, L., Giacovazzo, C., Polidori, G., Siliqi, D. and Spagna, R. (2007) IL MILIONE: a suite of computer programs for crystal

structure solution of proteins. *Journal of Applied Crystallography*, **40**, 609–613.

Černý, P., Chapman, R., Schreyer, W., Ottolini, L., Bottazzi, P. and McCammon, C.A. (1997) Lithium in sekaninaite from the type locality Dolni Bory, Czech Republic. *The Canadian Mineralogist*, **35**, 167–173.

Cesare, B., Maineri, C., Baron Toaldo, A., Pedron, D. and Acosta Vigil, A. (2007) Immiscibility between carbonic fluids and granitic melts during crustal anatexis: a fluid and melt inclusion study in the enclaves of the Neogene Volcanic Province of SE Spain. *Chemical Geology*, **237**, 433–449.

Cohen, J.P., Ross, F.K. and Gibbs, G.V. (1977) An X-ray and neutron diffraction study of hydrous low cordierite. *American Mineralogist*, **62**, 67–78.

Della Ventura, G., Bellatreccia, F., Cesare, B., Harley, S. and Piccinini, M. (2009) FTIR microspectroscopy and SIMS study of water-poor cordierite from El Hoyazo, Spain: Application to mineral and melt devolatilization. *Lithos*, **113**, 498–506.

Della Ventura, G., Bellatreccia, F., Marcelli, A., Cestelli Guidi, M., Piccinini, M., Cavallo, A. and Piochi, M. (2010) FTIR imaging in Earth Sciences. *Analytical and Bioanalytical Chemistry*, **397**, 2039–2049.

Della Ventura, G., Radica, F., Bellatreccia, F., Cavallo, A., Capitelli, F. and Harley, S. (2012) Quantitative analysis of H_2O and CO_2 in cordierite using polarized FTIR spectroscopy. *Contributions to Mineralogy and Petrology*, **164**, 881–894.

Duisenberg, A.J.M., Kroon-Batenburg, L.M.J. and Schreurs, A.M.M. (2003) An intensity evaluation method: EVAL-14. *Journal of Applied Crystallography*, **36**, 220–229.

Geiger, C.A. and Kolesov, B.A. (2002). Microscopic–macroscopic relationships in silicates: examples from IR and Raman spectroscopy and heat capacity measurements. Pp. 347–387 in: *Energy Modelling in Minerals* (C.-M. Gramaccioli, editor). European Notes in Mineralogy, **4**. Eötvös University Press, Budapest.

Goldman, D.S., Rossman, G.R. and Dollase, W.A. (1977) Channel constituents in cordierite. *American Mineralogist*, **62**, 1144–1157.

Gottesmann, B. and Förster, H.J. (2004) Sekaninaite from the Satzung granite (Erzgebirge, Germany): magmatic or xenolithic? *European Journal of Mineralogy*, **16**, 483–491.

Grapes, R., Korzhova, S., Sokol, E. and Seryotkin, Y. (2010) Paragenesis of unusual Fe-cordierite (sekaninaite)-bearing paralava and clinker from the kuznetsk coal basin, Siberia, Russia. *Contributions to Mineralogy and Petrology*, **162**, 253–273.

Guastoni, A., Demartin, F. and Pezzotta, F. (2004) Sekaninaite delle pegmatiti granitiche di Feriolo e Baveno (VB). *Atti della Società Italianadi Scienze Naturali e Museo Civico di Storia Naturale Milano*, **145**, 59–68.

Gunter, M.E., Bandli, B.R., Bloss, F.D., Evans, S.H., Su, S.C. and Weaver, R. (2004) Results from a McCrone Spindle Stage Short Course, a new version of EXCALIBR, and how to build a spindle stage. *Microscope*, **52**, 23–39.

Gunter, M.E., Downs, R.T., Bartelmehs, K.L., Evans, S.H., Pommier, C.J.S., Grow, J.S., Sanchez, M.S. and Bloss, F.D. (2005) Optic properties of centimeter-sized crystals determined in air with the spindle stage using EXCALIBRW. *American Mineralogist*, **90**, 1648–1654.

Hawthorne, F.C. and Černý, P. (1977) The alkali-metal positions in Cs-Li beryl. *The Canadian Mineralogist*, **15**, 414–421.

Herzberg, G. (1956) *Infrared and Raman Spectra of Polyatomic Molecules*. D. Van Nostrand Company, New York.

Hochella, M.F. Jr., Brown, G.E. Jr., Ross, F.K. and Gibbs, G.V. (1979) High-temperature crystal chemistry of hydrous Mg- and Fe-Cordierite. *American Mineralogist*, **64**, 337–351.

Khomenko, V.M. and Langer, K. (2005). Carbon oxides in cordierite channels: determination of CO_2 isotopic species and CO by single crystal IR spectroscopy. *American Mineralogist*, **90**, 1913–1917.

Kolesov, B.A. and Geiger, C.A. (2000) Cordierite II: the role of CO_2 and H_2O. *American Mineralogist*, **85**, 1265–1274.

Libowitzky, E. and Rossman, G.R. (1996) Principles of quantitative absorbance measurements in anisotropic crystals. *Physics and Chemistry of Minerals*, **23**, 319–327.

Libowitzky, E. and Rossman, G.R. (1997) An IR absorption calibration for water in minerals. *American Mineralogist*, **82**, 1111–1115.

Malcherek, T., Domeneghetti, M.C., Tazzoli, V., Ottolini, L., McCammon, C. and Carpenter, M.A. (2001) Structural properties of ferromagnesian cordierites. *American Mineralogist*, **86**, 66–79.

Nonius (1998) COLLECT. Nonius BV, Delft, The Netherlands.

Orlandi, P. and Pezzotta, F. (1994) La sekaninaite dei filoni pegmatitici elbani. *Atti della Società Toscana di Scienze Naturali, Memorie*, **100**, 85–91.

Paukov, I.E., Kovalevskaya, Y.A., Rahmoun, N.-S. and Geiger, C.A. (2007) Heat capacity of synthetic hydrous Mg-cordierite at low temperatures: thermodynamic properties and the behavior of the H_2O molecules in selected hydrous micro and nanoporous silicates. *American Mineralogist*, **92**, 388–396.

Ryback, G., Nawaz, R. and Farley, E. (1988) Seventh supplementary list of British Isles Minerals (Irish). *Mineralogical Magazine*, **52**, 267–274.

Sekanina, J. (1928) Minerals of Moravian pegmatites. *Acta Musei Moraviae, Scientie Naturales*, **26**,

113–224 (in Czech).

Selkregg, K.R. and Bloss, F.D. (1980). Cordierites: compositional controls of Δ, cell parameters, and optical properties. *American Mineralogist*, **65**, 522–533.

Sharygin, V.V., Sokol, E.V. and Belakovskii, D.I. (2009) Fayalite-sekaninaite paralava from the Ravat coal fire (central Tajikistan). *Russian Geology and Geophysics*, **50**, 703–721.

Sheldrick, G.M. (2008) A short history of SHELX. *Acta Crystallographica.* **A64**, 112–122.

Sherriff, B.L., Grundy, H.D., Hartman, J.S., Hawthorne, F.C. and Černý, P. (1991) The incorporation of alkalis in beryl, a multinuclear MAS-NMR and crystal structure study. *The Canadian Mineralogist*, **29**, 271–285.

Staněk, J. and Miškovský, J. (1964) Iron-rich cordierite from the Dolní Bory pegmatite. *Casopis pro mineralogii a geologii*, **9**, 191–192 (in Czech).

Staněk, J. and Miškovský, J. (1975) Sekaninaite, a new mineral of the cordierite series, from Dolní Bory, Czechoslovakia. *Scripta Facultatis Scientiarum Naturalium Universitatis Purkynianae Brunensis; Geologia 1*, **5**, 21–30.

Su, S.C., Bloss, F.D. and Gunter, M.E. (1978) Procedures and computer programs to refine the double variation method. *American Mineralogist*, **72**, 1011–1013.

Thompson, P., Harley, S.L. and Carrington, D.P. (2001) The distribution of H_2O-CO_2 between cordierite and granitic melt under fluid-saturated conditions at 5 kbar and 900ºC. *Contributions to Mineralogy and Petrology*, **142**, 107–118.

Yakubovich, O.V., Massa, W., Pekov, I.V., Gavrilenko, P.G. and Chukanov, N.V. (2004) Crystal structure of the Na-, Ca-, Be-cordierite and crystallochemical regularities in the cordierite–sekaninaite series. *Crystallography Reports*, **49**, 953–963.